ELSEVIER

A structure study of the electroless deposition of Au on Si(1 1 1):H

S. Warren [a], A. Reitzle [b], A. Kazimirov [c], J.C. Ziegler [b], O. Bunk [d], L.X. Cao [a],
F.U. Renner [a], D.M. Kolb [b], M.J. Bedzyk [e,f], J. Zegenhagen [a,*]

[a] *ESRF, Avenue Jules Horowitz, BP-220, F-38043 Grenoble Cedex, France*
[b] *Abteilung Elektrochemie, Universität Ulm, D-89069 Ulm, Germany*
[c] *CHESS, Wilson Laboratory, Cornell University, Ithaca, NY 14853, USA*
[d] *II. Institut für Experimentalphysik, Universität Hamburg, D-22761 Hamburg, Germany*
[e] *Department of Materials Science and Engineering and Materials Research Center, Northwestern University, Evanston, IL 60208, USA*
[f] *Materials Science Division, Argonne National Laboratory, Argonne, IL 60439, USA*

Abstract

Electroless deposition of gold in monolayer amounts on hydrogen terminated Si(1 1 1) was studied by a variety of structure sensitive techniques. Rutherford back scattering data revealed a linear relationship between the Au coverage and the concentration of the Au solution used for deposition. Atomic force microscopy and surface X-ray diffraction studies indicated cluster formation, with the Au(1 1 1) face epitaxially aligned to the Si(1 1 1):H substrate. However, X-ray standing wave experiments at coverage below one monolayer suggested the formation of a gold layer. Both clusters and isolated Au atoms appear to be present at all coverages, which is explained by the formation of type of Au 'wetting layer', in addition to cluster formation which increases as the coverage increases. © 2001 Elsevier Science B.V. All rights reserved.

1. Introduction

Noble-metal deposition on Si has been extensively studied due to an interest in the fundamental aspects of metal growth as well as the importance of metal/silicon interfaces in microelectronics. In addition to the possible formation of silicides, which occurs with the deposition of certain noble metals [1–3], the growth mode of a metal can be influenced by many factors. Significant differences in the growth mode have been observed for hydrogen passivated Si surfaces versus bare Si surfaces [4]. The electrochemical deposition of Au is used to produce electrical and conductive coatings [5], or absorber layers in X-ray masks [6]. Noble metals can also contaminate the surfaces of Si wafers during cleaning and preparation for

* Corresponding author. Tel.: +33-476-882866; fax: +33-476-882160.

E-mail address: zegenhagen@esrf.fr (J. Zegenhagen).

manufacturing. Thus an understanding of the structure of metal/semiconductor interfaces is very important, in particular in connection with wet chemical procedures.

The electroless deposition used here operates at ambient temperatures and pressures, and represents a simple and economic method of metal deposition onto Si surfaces. A study of the structure of the metal/semiconductor interface produced could therefore provide information regarding both the fundamental growth mechanism, and the viability of such a technique for manufacturing processes in microelectronics.
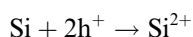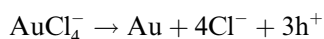
2. Experimental

In this study one-side polished n-Si(1 1 1) samples, phosphorus-doped, 1–20 Ω cm (approximately 10^{15} cm^{-3} doping density) with a low miscut angle of about 0.1° were used (supplied by Wacker Siltronic AG, Burghausen, Germany). First, the samples were degreased for about 2 h by refluxing in isopropanol. Then they were cleaned following the RCA method [7]: i.e. boiling in a 1:1:5 volume mixture of NH$_3$, H$_2$O$_2$ and H$_2$O, and afterwards in a 1:1:5 volume mixture of HCl, H$_2$O$_2$ and H$_2$O at about 80 °C. Samples prepared in this way can be stored under ultrapure water and in the dark for about three days without risk of new contamination.

Prior to the deposition of Au, the Si samples were immersed for 1 min into 50% HF to remove the oxide created by the preparation, and then for 3 min in 40% NH$_4$F solution. This procedure is known to result in well-defined monohydride-terminated Si(1 1 1) surfaces with large, atomically flat terraces [8–10].

Electrochemical deposition of metals onto the H-terminated n-Si(1 1 1) electrodes can occur in principle in two different ways: potential-controlled or electroless. In potential-controlled experiments, an appropriate voltage is applied to the electrode. This facilitates the transfer of electrons from the electrode conduction band to the overlapping (i.e., isoenergetic) metal acceptor states (see the Gerischer model of ionic redox states in solution [11,12]). However, with noble metals in

solution (i.e. metals with very positive equilibrium potentials such as Au, Ag or Pt), there is a strong overlap between the acceptor state in solution and the semiconductor valence band. Therefore, electroless deposition occurs via hole injection into the semiconductor valence band. As a consequence, the semiconductor is oxidised (and etched, it depends on the semiconductor) as the noble metal is deposited [13,14]. This electroless deposition method was used to deposit Au on hydride terminated Si(1 1 1), and the net process involves deposition of Au, and dissolution of Si:

$$AuCl_4^- \rightarrow Au + 4Cl^- + 3h^+$$

$$Si + 2h^+ \rightarrow Si^{2+}$$

In these experiments, all electrolytes were prepared from high-purity chemicals (supplied by Merck Eurolabs, Flucka and Aldrich) and Milli-Q-water (18.2 MΩ cm, total organic carbon = 3 ppb). To deposit the gold, the clean, H-terminated Si sample was simply dipped into a solution of 0.1 M HCl, 5 vol%HF and 1 μm–1 mM K[AuCl$_4$] for a set amount of time.

The H-terminated Si surfaces are hydrophobic, as observed when rinsing in ultrapure water. Immediately after deposition of Au, the samples still exhibit hydrophobic behaviour, indicating that the H passivation remains intact over large areas of the sample. Any oxidation, or contamination of the samples would be readily observed by a change in the hydrophobic nature of the H-terminated and Au-H:Si(1 1 1) samples.

Rutherford back scattering (RBS) was used to calculate the amount of Au on the surface, which is dependent on the K[AuCl$_4$] concentration, and the sample exposure time to the solution. The coverage given here in monolayers (ML) is expressed with respect to the Si substrate, where 1 ML = 7.84×10^{14} atoms/cm^2.

All ex situ atomic force microscopy (AFM) experiments were performed in air with a Pico-SPM (Molecular Imaging Corporation, Tempe, USA) that operates in contact mode, using Si cantilevers (Park Ultralever 0.6 μm) with a spring constant of 0.31 N m^{-1} as specified by the manufacturer.

The surface X-ray diffraction (SXRD) experiments were also performed in air at the BW2

wiggler beamline at HASYLAB and at beamline ID32, ESRF, using a photon energy of 10 keV ($\lambda = 1.24$ Å). Data were recorded from the specular diffraction peaks, and also along the high symmetry in-plane directions. Both beamlines were equipped with four-circle diffractometers.

The X-ray standing wave (XSW) experiments were carried out at beamline X15A [15] of the National Synchrotron Light Source, Brookhaven National Laboratory, USA. The Si(1 1 1) reflection curve of the sample was obtained by changing the energy of the Si(1 1 1) monochromator tuned to 17.2 keV ($\lambda = 0.72$ Å), and the Si(2 2 0) reflection at 12.5 keV ($\lambda = 0.992$ Å) using a Ge monochromator. The measurements were performed in air, and the Au fluorescence was recorded using a lithium drifted silicon solid-state detector.

3. Results

The RBS data obtained in Stuttgart indicated a linear relationship between the Au concentration on the surface and the $[AuCl_4]^-$ solution concentration for a given exposure time of the Si sample (30 s). Subsequent sample preparation was carried out using a constant exposure time and varying the concentration of the Au solution, in order to deposit the desired amount of Au. For the following results, the concentration of Au on the surface was calibrated from the RBS analysis, and is given in monolayers, where 1 ML is defined as 7.84×10^{14} atoms/cm^2, and exposure to a 1 μM $[AuCl_4]^-$ solution deposits approximately 0.03 ML Au on the Si substrate. Unfortunately, the quantitative RBS analysis cannot be used for the samples prepared for AFM measurements, as those were prepared by varying the dipping time in the $[AuCl_4]^-$ solution.

3.1. Atomic force microscopy

In Fig. 1a, an ex situ AFM image of a monohydride-terminated n-Si(1 1 1) surface, prepared as described above, is shown. Typical features of this surface are atomically flat terraces separated by steps of 3.1 Å in height (the height of a Si-bilayer), with some triangular etch pits aligned along the

main crystallographic directions of the Si(1 1 1) substrate. The formation of these etch pits can be avoided by thoroughly de-aerating the NH_4F solution by bubbling Ar or N_2 through the solution [16]. The step density and the average size of the terraces are determined by the miscut of the wafer. In air, the H-termination was stable for hours, and no change in the surface morphology (for instance, as a result of silicon oxidation) could be observed with the AFM. These well-defined surfaces were used for the gold deposition experiments.

Fig. 1 shows three AFM images of surfaces which had been exposed for 1 s (Fig. 1b), 5 s (Fig. 1c) and 30 s (Fig. 1d) to the 1 μM $K[AuCl_4]$ plating solution. The images still reveal the typical features of a H-terminated Si(1 1 1) surface: namely large, atomically flat terraces and Si-bilayer steps. The triangular etch pits can also be recognised. There is no significant change of the Si(1 1 1) surface observed due to the dissolution of Si from the oxidising/etching procedure in the $K[AuCl_4]$ solution. However, all three pictures show surfaces with Au coverages less than 0.02 ML, corresponding to a dissolution of 0.03 ML of Si, and such changes would be too small to be distinguished in the AFM images. In addition, one can clearly see three-dimensional (3D) Au clusters (the white spots in Fig. 1b–d). A 3D growth mechanism was reported for electroless deposition of Au on an atomically rough, HF-etched n-H:Si(1 1 1) surface [17–19], and for the electrodeposition of Au onto n-Si(1 0 0) in alkaline solution [20–22]. The growth of Au on H:Si(1 1 1)-(1 × 1) during vapour deposition in UHV is also 3D, as opposed to two-dimensional (2D) on the bare Si(1 1 1)-(7 × 7) [4]. In our case, gold clusters can be found distributed randomly on terraces as well as at kink-sites and there seems to be no preferential nucleation sites for the electroless deposited Au. The average size and number per μm^2 of the clusters for each sample is given in Table 1. As can be seen easily, the longer the dipping time, the larger the size and the larger the average number of the nuclei. The limited resolution of the AFM tip makes the determination of the real size of the nuclei difficult, and this prevents any quantitative analysis of the proportion of gold clusters on the surface. Imaging samples with coverages much higher than 0.02 ML has not been
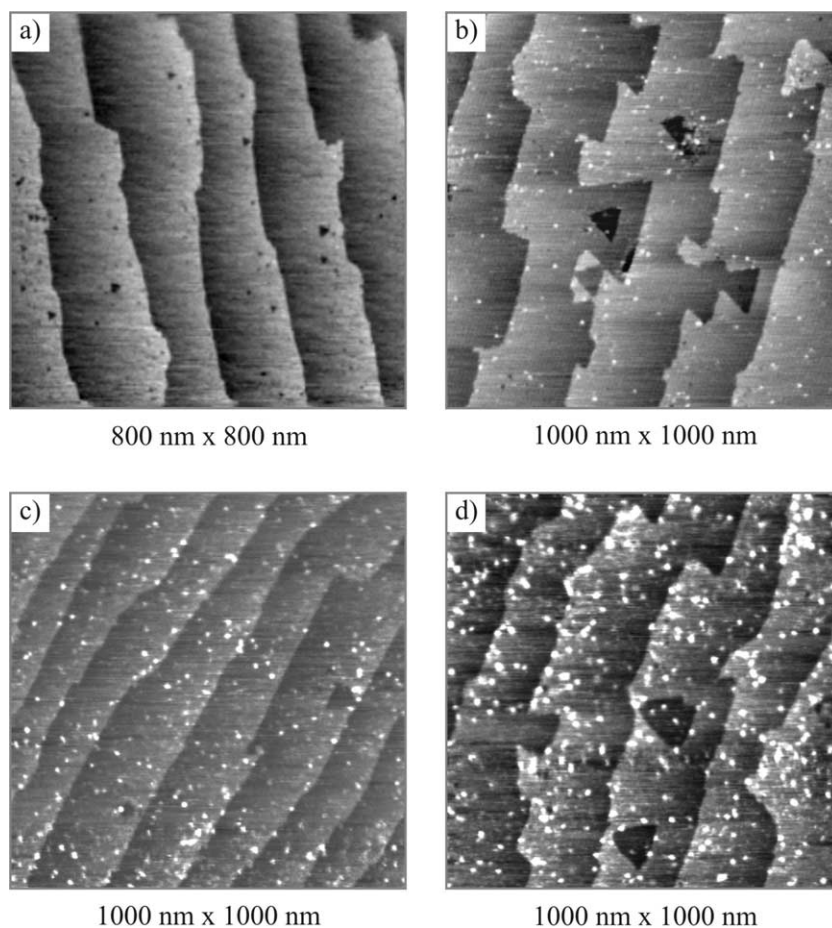
Fig. 1. Ex situ AFM image of the monohydride-terminated *n*-Si(1 1 1) surface before Au deposition (a), after 1 s, (b) 5 s (c) and 30 s (d) of exposure to the 1 μM K[AuCl₄] plating solution.

possible to date, as after the electroless Au deposition the surface seems to be too rough to be imaged by contact-mode AFM.

3.2. X-ray diffraction

For the X-ray diffraction (XRD) analysis, we adopt the hexagonal surface co-ordinate system for the Si substrate ($a_{Si} = 5.431$ Å), using reciprocal lattice vectors $\mathbf{a}^*$, $\mathbf{b}^*$ and $\mathbf{c}^*$, where $\gamma(\mathbf{a}^*, \mathbf{b}^*) = 60°$, and $\beta(\mathbf{a}^*, \mathbf{c}^*) = \alpha(\mathbf{b}^*, \mathbf{c}^*) = 90°$. Surface XRD measurements were performed on samples with a range of Au deposition concentrations from 0.019 to 35 ML, with all samples being freshly prepared immediately prior to measurement, to reduce any

Table 1
Average height and number of gold clusters on H:Si(1 1 1) for three different times of exposure to the K[AuCl₄] plating solution, measured from AFM images

	Exposure time to solution (s)		
	1	5	30
Cluster height (Å)	7.5	9.5	12.5
Number of clusters (per μm⁻²)	350	430	540

degradation effects. At lower concentrations of Au, the surface diffraction peaks were not of high enough intensity to be observed. Two sets of data are shown (for the 1.9 and 15.3 ML samples) to illustrate the behaviour of the Au-H:Si(1 1 1) system.
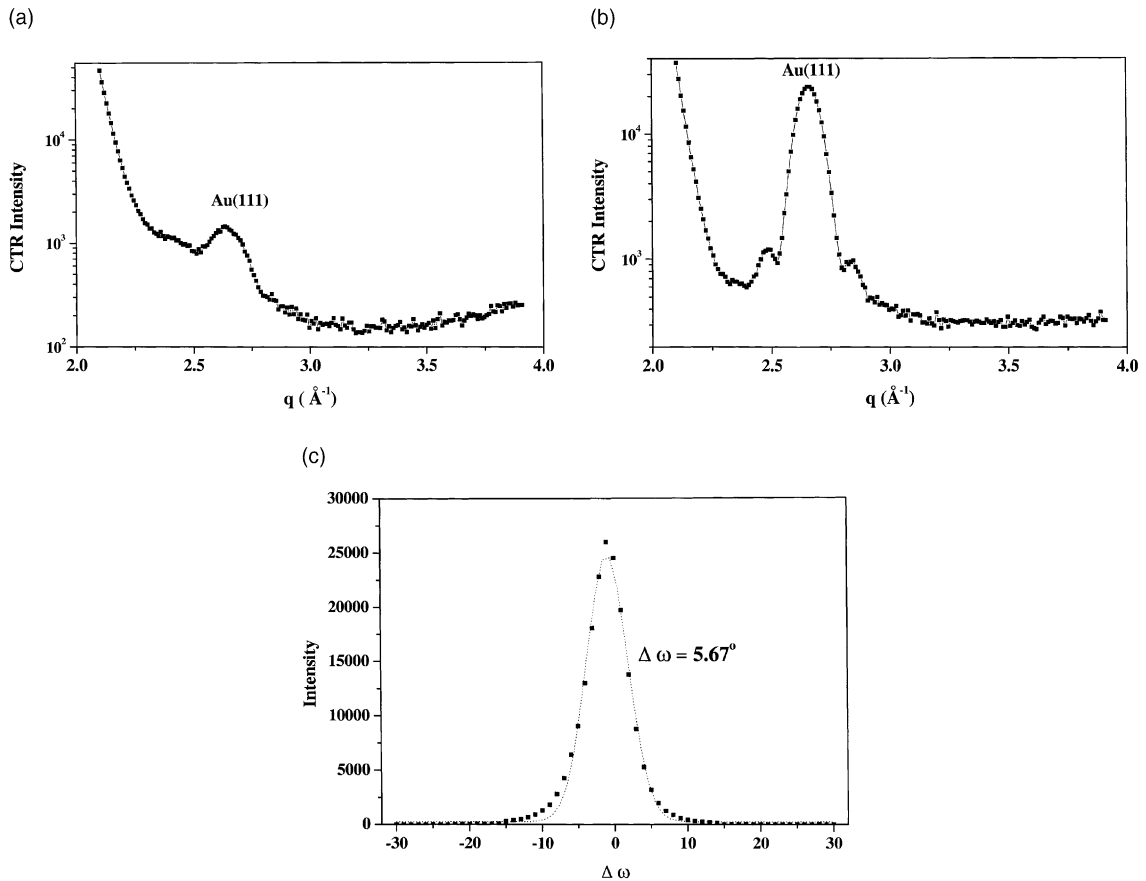
(a)

(b)

(c)

Fig. 2. Specular $q_\perp$ scans along [0 0 l] direction of Si after electroless gold deposition; (a) 1.9 ML gold, (b) 15.3 ML gold, (c) ω scan recorded from the 15.3 ML sample (■), with a curve fit to the data (- - -) showing FWHM $\Delta\omega = 5.67°$.

Fig. 2a and b shows the q scans recorded along the [0 0 l] direction (i.e. the specular scan) for samples of 1.9 and 15.3 ML Au. The Au(1 1 1) peak is clearly seen, indicating that (1 1 1) planes of gold grow parallel to the Si(1 1 1) planes. No other diffraction peaks due to gold are seen in the specular direction, indicating that the Au(1 1 1) growth direction is highly preferred, and that the substrate–gold interaction is strong. An estimate of the thickness of the gold layers (from the width of the Au(1 1 1) peak) indicates the (nominally) 1.9 ML Au sample consists of Au clusters of an average thickness of 16 ML. For the 15.3 ML sample (Fig. 2b), Pendellösung fringes are observed, indicating that the island thickness (approximately 23 ML) is well defined. The fact that islands or

clusters of Au have formed on the sample surface yields important evidence of the growth mechanism.

The ω scan (or rocking curve) of the Au(1 1 1) peak from the 15.3 ML sample is shown in Fig. 2c. A fit to the data shows the FWHM to be around 5°, indicating a low mosaic spread for the Au(1 1 1) islands on the Si(1 1 1) surface.

In plane surface XRD data recorded from both samples are shown in Fig. 3 for the [1,0] direction. For both samples, the Au(2 2 0) peak is seen, and for the higher coverage sample, the Au(2 2 2) peak is also observed. An omega scan of the Au(2 2 0) peak from the 15.3 ML sample is shown in Fig. 3c, and indicates the epitaxial ordering of Au on the H:Si(1 1 1) substrate. Maxima are seen at
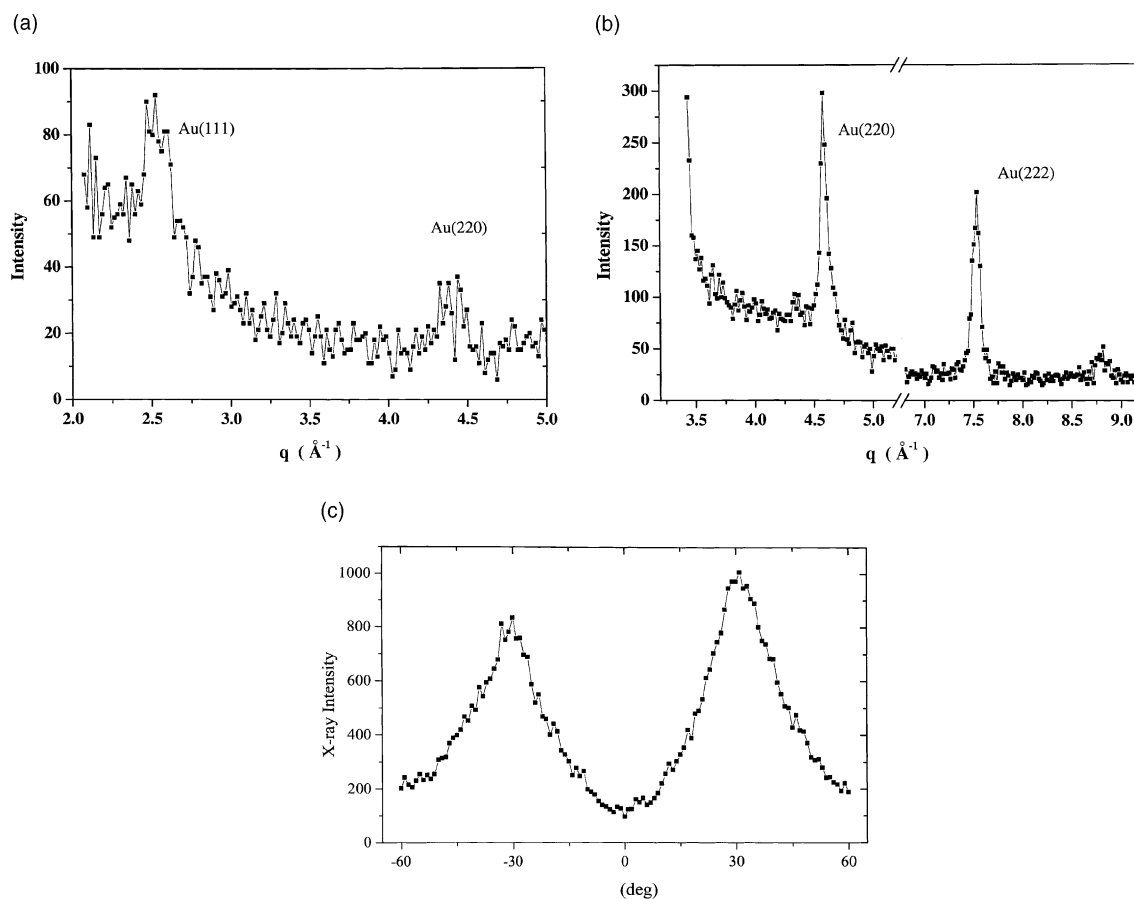
(a)

(b)

(c)

Fig. 3. In-plane $q_\parallel$ scans along [1,0] direction of Si after electroless gold deposition; (a) 1.9 ML gold, (b) 15.3 ML gold, clearly showing the Au(2 2 0) peak, (c) ω scan recorded from the Au(2 2 0) peak of the 15.3 ML sample showing maxima at $\Delta\omega = \pm30°$.

$\Delta\omega = \pm30°$, indicating a strong preference for alignment of the Au clusters with the high symmetry H = K axes of the Si substrate.

Surface XRD data recorded along the [1,1] direction are shown in Fig. 4a and b, where again, the Au(2 2 0) peak is clearly seen. Omega scans of this peak (Fig. 4c) indicate the alignment along the high symmetry axes of the Si(1 1 1) substrate. The most prominent peak is at $\Delta\omega = \pm30°$, (along the H and K axes), but there are also smaller peaks at $\pm11°$ and $\pm48°$, indicating that there are other stable alignments directions adopted by a minority of the gold islands.

The values of the Au d-spacings, d_{Au}, as calculated from the peak positions in the SXRD measurements are given in Table 2. There seems to be

little difference between the low coverage, and high coverage Au species, and both agree well with the theoretical values for bulk Au. This suggests that there is little strain in the Au islands. The majority species of Au clusters grow with the Au(1 1 1) planes parallel to the Si(1 1 1) planes. A minority of clusters also grow with the Au(1 1 1) planes in-plane for the higher coverage sample, as a small Au(1 1 1) peak is seen in the radial scan (Fig. 4). Here the d spacings are slightly larger than the theoretical values, perhaps reflecting that this orientation is not the preferred one, and some distortion of the Au lattice occurs. Measurements of samples over the range of concentration 0.019–35 ML show essentially the same behaviour: a gradual increase in the thickness of the Au islands with
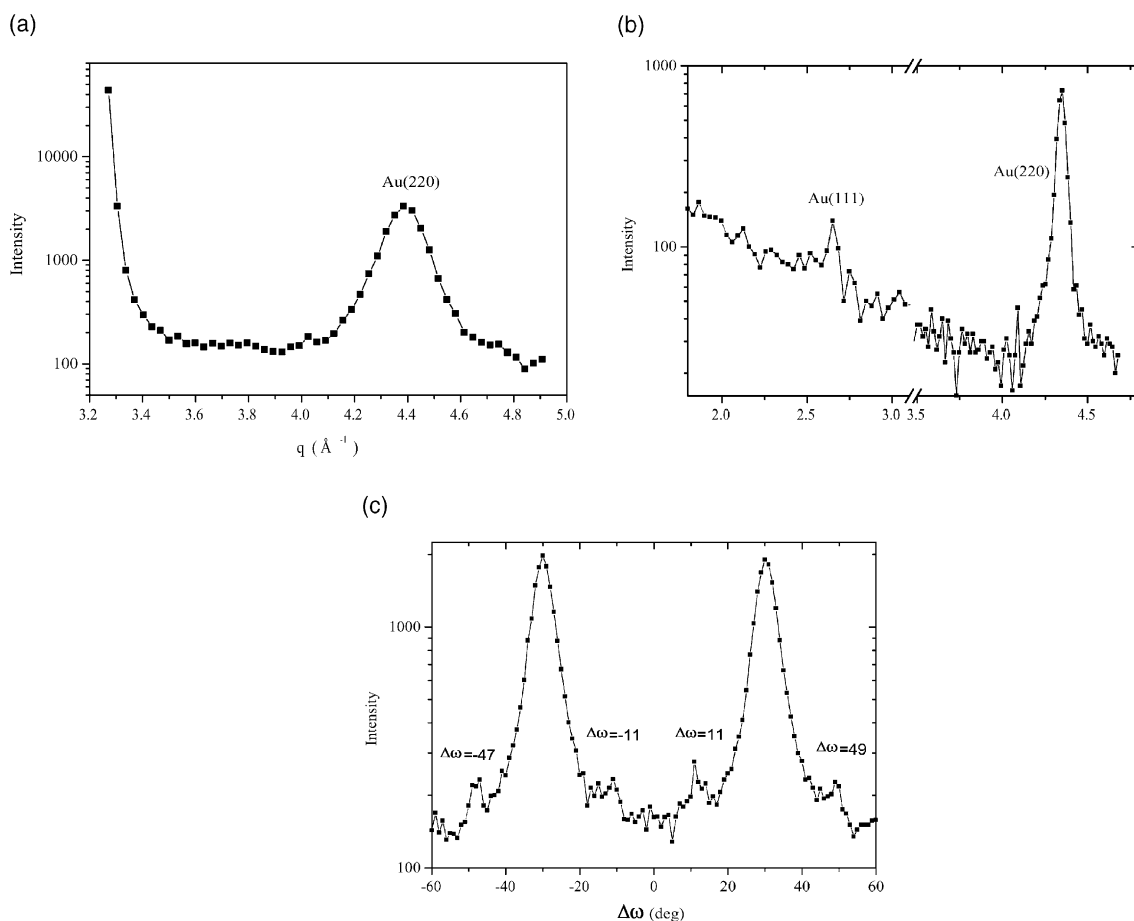
(a)

(b)

(c)

Fig. 4. In-plane $q_\parallel$ scans along [1,1] direction of Si after electroless gold deposition; (a) 1.9 ML gold, (b) 15.3 ML gold, (c) ω scan recorded from the Au(2 2 0) peak of the 1.9 ML sample showing maxima at $\Delta\omega = \pm30°$ and at $\pm11°$, $\pm48°$.

Table 2
Au cluster d-spacings, as determined from the SXRD data, and a comparison with the theoretical d-spacings for bulk Au

	Sample		
	1.9 ML d (Å)	15.3 ML d (Å)	d (Å)$_{theory}$
Au(1 1 1) specular	2.385	2.357	2.355
Au(2 2 2) specular		1.197	1.177
Au(2 2 0) [1,0]	1.446	1.444	1.442
Au(2 2 0) [1,1]	1.4319	1.444	1.442
Au(1 1 1) [1,0]		2.373	2.355
Au(2 2 2) [1,0]		1.124	1.177

increasing Au deposition, all aligned epitaxially to the Si(1 1 1) substrate, with the Au(1 1 1) growth planes parallel to the substrate.

The crystal truncation rod scattering of both samples was recorded, and an example is shown in Fig. 5. The rods were similar for both coverages, with the exception of the scaling, indicating that a 3D structure is formed by the electroless deposition of Au on H:Si(1 1 1) samples. Furthermore, we compared the (1.34, 0, l) crystal truncation rod (CTR) of the 1.9 ML sample (open triangles) with the (1.34, 0, l) CTR of an as prepared H-terminated n-Si(1 1 1) surface (open circles) to get information about the roughening of the Si substrate during the gold deposition process. In the region between the Bragg reflections at $l = 1/3$ and $l = 4/3$, the scattered intensity is strongly dependent on the surface roughness. By fitting the
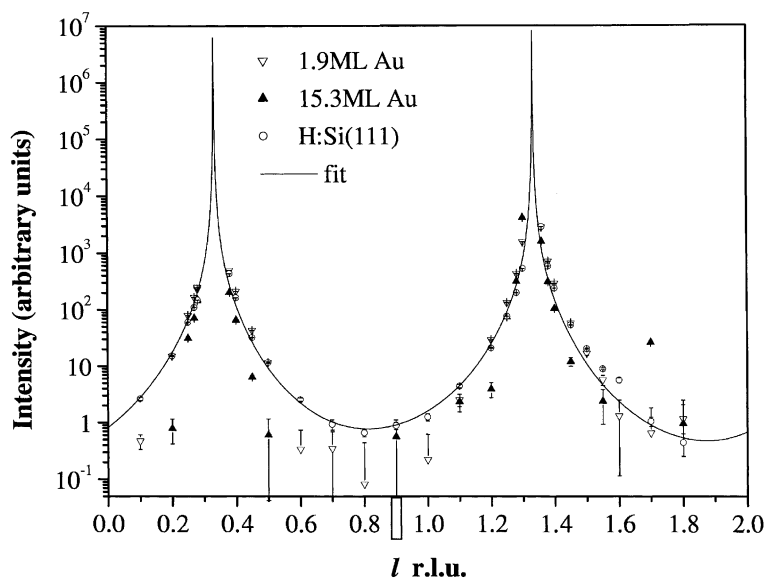
Fig. 5. Crystal truncation rod recorded from the 1.9 and 15.3 ML gold sample and the bare H:Si(1 1 1) surface along [1.34, 0, l]. The fit to the bare H:Si data is shown as a solid line.

experimental data to the model by Robinson [23], one can derive a β value, which describes the occupancy β^n of the surface level n. From this β value, a root-mean-square value of the surface roughness σ_{RMS} can be calculated:

$$\sigma_{RMS} = \frac{\sqrt{\beta}}{1-\beta} d_\perp$$

where $d_\perp$ is the distance between the Si(1 1 1) planes ($d_\perp = 3.14$ Å). A significant increase in the surface roughness after the gold deposition can be seen: i.e., the scattering intensity for the Au covered surface in the region between the Bragg reflections is much smaller. The β values for the Au-free and the Au-covered surfaces are $\beta = 0.283$ and $\beta = 0.732$ respectively, and the corresponding σ_{RMS} increases from 2.3 to 10 Å.

Evidence for 3D structures has also been found for other metals deposited on monohydride Si surfaces e.g. for Pb [24] and Ag [25], whereas deposition onto bare Si often results initially in a 2D structure. The hydride termination appears to make the Au more mobile on the surface, allowing the formation of clusters and islands. The SXRD data therefore seems to confirm the AFM obser-

vations, and indicates a 3D or Volmer–Weber growth mode of Au accompanied by a significant roughening of the Si(1 1 1) surface.

3.3. X-ray standing wave

The XSW data recorded from samples over a range of Au coverages are shown in Fig. 6. At higher coverages (e.g. Fig. 6c and e) the coherent fraction F is very low, indicating a large degree of incoherence of the Au atoms with respect to the substrate atomic planes. The coherent fraction F is significant at low coverages, indicating a large proportion of the Au deposited occupies ordered sites. For both reflections, the coherent fraction F decreases with coverage, though the coherent position P remains roughly constant, as shown in Fig. 7a. The coherent coverage (shown in Fig. 7b) indicates the amount of the ordered phase on the surface, with increasing Au coverage. This clearly increases as the amount of Au on the surface increases, indicating that the *absolute* amount of Au occupying this preferred site increases with coverage. However, the *relative* proportion of the total Au on the surface occupying this site is decreasing,
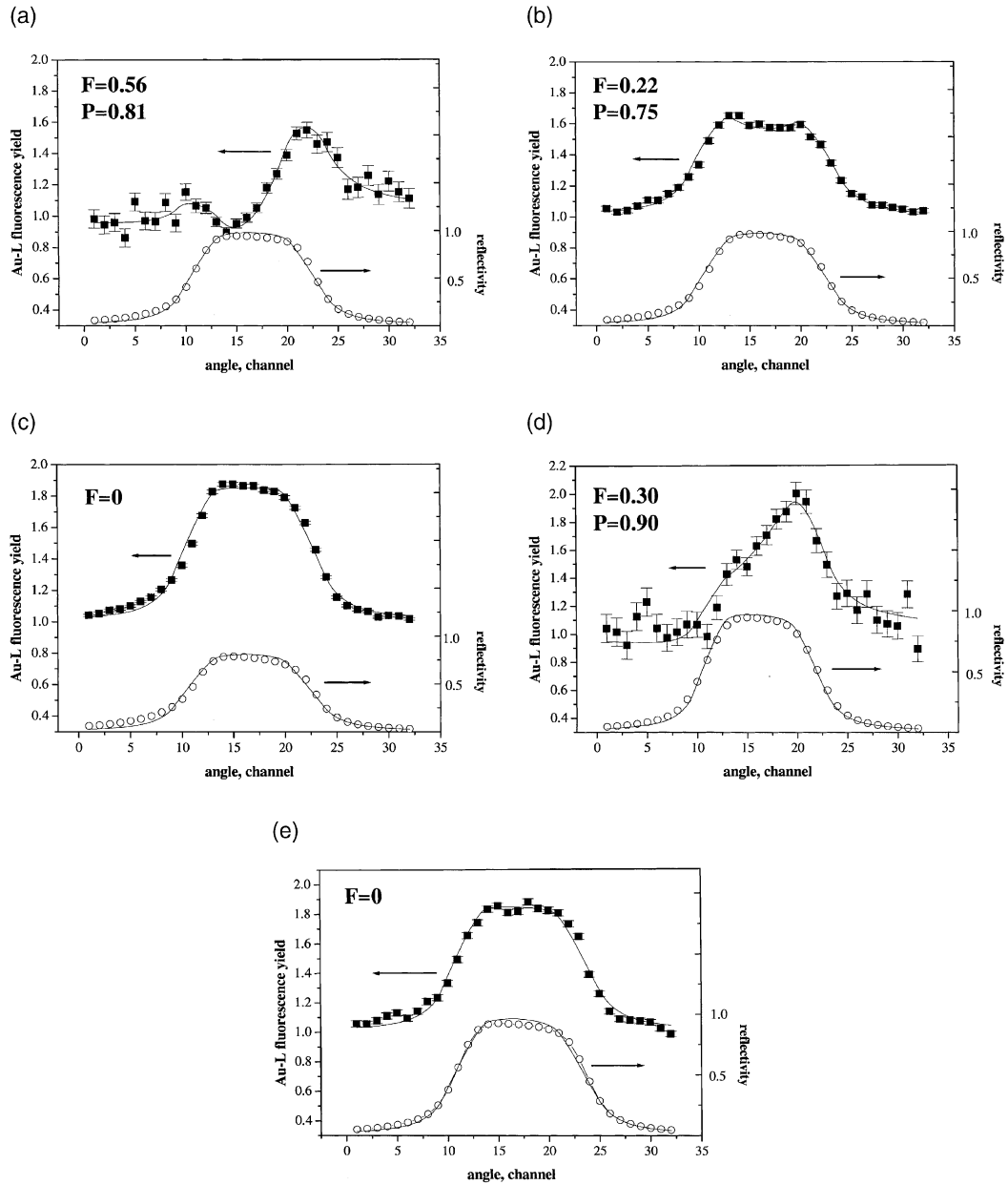
Fig. 6. XSW measurements recorded over a range of Au coverages, after calibration by RBS. Reflectivity data (○) and the X-ray standing wave (■) are shown for each sample, together with the coherent position P, and coherent fraction F calculated from curve fitting to the XSW data. The XSW data were recorded for the Si(1 1 1) reflection (at 17.2 keV) (a–c), or the Si(0 2 2) reflection (d, e). The nominal amounts of Au on the surface are (a) 0.03 ML, (b) 1.88 ML, (c) 15.2 ML, (d) 0.10 ML, (e) 0.63 ML.

as more gold is deposited. The possible position of the Au site can be triangulated from the coherent positions for the Si(1 1 1) and Si(0 2 2) reflections, and is illustrated in Fig. 8.

In comparison, XSW analysis of the adsorption of 0.3–0.4 ML Au on bare Si(1 1 1) in UHV has been carried out by Durbin et al. [26] both immediately after vacuum deposition, and after
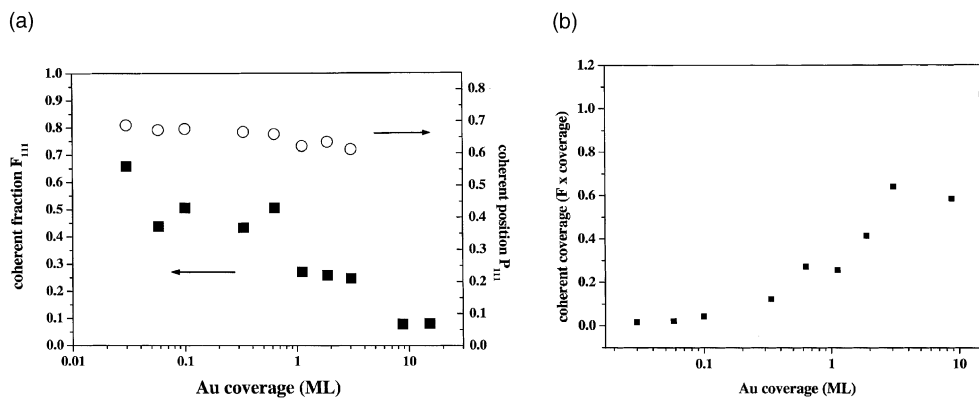
(a)   (b)

Fig. 7. (a) Coherent fraction, F, and coherent position, P, for the (1 1 1) XSW reflection, as a function of coverage. (b) The coherent coverage of the Au-H:Si(1 1 1) sample, as a function of Au deposited.
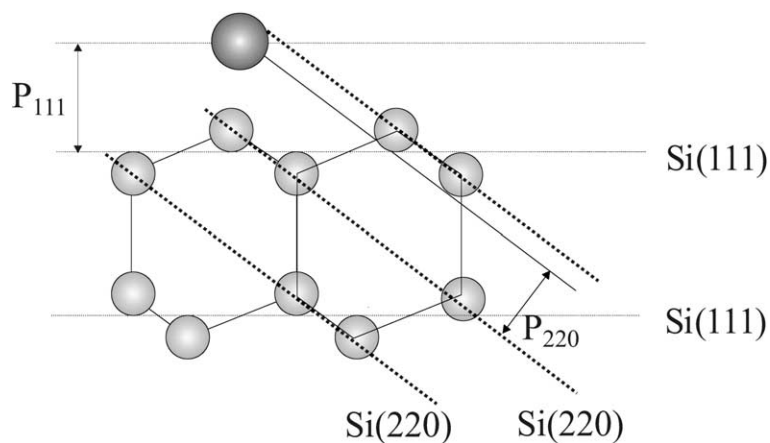

Fig. 8. Position of Au atoms on the H:Si(1 1 1) sample, from XSW data. For the (1 1 1) reflection, $P = 0.81$, and for the (0 2 2) reflection, $P = 0.90$. The triangulated position is shown.

annealing the Si substrate. The annealed surface gave a highly ordered Au layer, with a coherent fraction of 80–90%. However, the 'as prepared' sample shows a coherent fraction of around 8%. This is in contrast to our results, from deposition of Au on the monohydride Si(1 1 1) surface. For the electroless deposition, even at low coverages, and with no further sample treatment, the coherent fraction F is above 50%, suggesting that the hydride termination allows the deposited Au atoms to migrate and occupy the more favourable surface sites. The site occupied by the Au on the H:Si(1 1 1) surface also appears to be different. The UHV study suggests that the annealed Au is embedded in the hollow sites between the top two Si

atomic planes, which relax outwards to incorporate Au. In contrast, our data points to a site directly above the Si atoms as shown in Fig. 9. Clearly, the hydride termination has a significant effect on both the kinetics and thermodynamic stability of the most preferred site.

XSW measurements can determine only the relative position of the Au atoms with respect to the Si(1 1 1) or Si(0 2 2) planes, and cannot distinguish between an Au atom lying on top of the H:Si(1 1 1) surface, or one that has diffused into the top layers of the substrate, as occurs for Fe deposition on H:Si(1 1 1) [1]. An 'embedded' Au layer below the topmost Si plane could also generate the same coherent position with respect to the Si
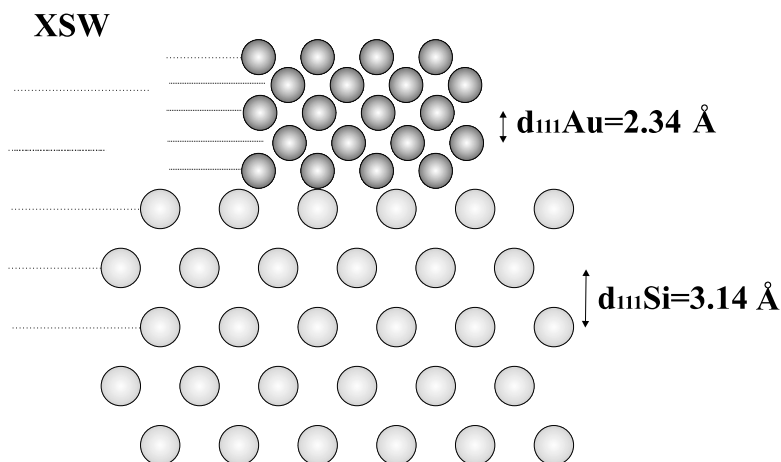
XSW

$d_{111}Au = 2.34$ Å

$d_{111}Si = 3.14$ Å

Fig. 9. As the 3D Au islands grow on the Si(1 1 1) substrate, the Au atoms no longer occupy coherent positions with respect to the Si(1 1 1) atomic plane.

substrate planes, and cannot be ruled out from our data. However, this proposed ordered coverage of Au with respect to the Si(1 1 1) substrate appears to be at odds with the AFM and SXRD data, which indicate clusters or Volmer–Weber growth on the sample surface. A description of Au deposition on H:Si(1 1 1), which reconciles these two models, will be outlined below.

4. Discussion and conclusions

The AFM images and the SXRD data from the Au-H:Si(1 1 1) system point to cluster formation from the very beginning, with the Au islands aligned along the high symmetry axes of the substrate. In addition, the Au islands appear to grow with the (1 1 1) Au atomic planes parallel to those of the Si(1 1 1) substrate, with only a small mosaic spread (indicating the 'tilt' of the Au(1 1 1) planes away from the epitaxial orientation). These results agree well with previous work on Au deposition on monohydride Si(1 1 1) [17–19], and suggest that the hydride termination causes a 3D or Volmer–Weber growth mode.

However, the XSW data seem to indicate a 2D growth mechanism, resulting in a significant proportion of the deposited Au atoms occupying sites 'atop' Si atoms (either on the surface, or 'atop' the Si atom planes below the surface). This ordered

layer appears to be some sort of 2D 'wetting layer' within the surface region of the H:Si(1 1 1) sample. It is perhaps at first surprising that the electroless deposition should produce an ordered surface structure, with no further annealing or other sample treatment; but the hydride termination appears to make the gold atoms more mobile on the sample surface, and this would allow occupation of the most favoured sites.

The H:Si(1 1 1) surface surrounding the gold clusters is thought to become too rough during the Au deposition-Si dissolution process to allow observation of the 2D Au structure with AFM. A very flat substrate surface would be required to image this in AFM. The 'wetting layer' may also have an effect on the crystal truncation rods observed in XRD studies of the surface. However, the electroless deposition process involves etching of the Si substrate, and itself has a roughening effect. Therefore, samples with deposited gold are always 'roughened' as compared to the bare substrate. Thus, where the CTRs are most surface sensitive, between the integer *l*-points, it is impossible to differentiate the increase in roughness measured due to the etching of Si, from the roughness (if any) that would be introduced by the 2D ordered Au layer structure.

The growth mechanism therefore seems to be an ordered 2D layer of gold atoms at low coverage, with the Au atoms occupying the sites illustrated

in Fig. 8, though clusters are already present as observed in AFM. As the coverage increases, gold islands or clusters are increasingly formed on the surface of the H:Si(1 1 1), with the Au(1 1 1) atomic planes lying parallel to the substrate Si(1 1 1) planes. The orientation of the islands within the surface plane is also specific along the high symmetry H, K and H = K axes. As these islands are formed, the XSW technique can no longer identify the Au position, because the Au atom spacing within the gold island is not coherent with respect to the substrate atomic planes, as is illustrated in Fig. 9. As with other metals on Si [1,3,24], the hydride termination strongly influences the growth mechanism, making the Au atoms more mobile on the H:Si(1 1 1) surface.

5. Summary

The electroless deposition of Au on H:Si(1 1 1) forms an ordered 2D wetting layer at low coverages, with Au atoms 'atop' the Si position, as determined by XSW measurements. Au clusters, epitaxially aligned with the substrate, and present also at low coverages, are observed with AFM and SXRD, with cluster growth increasing as the coverage increases.

References

[1] M.G. Martin, J. Avila, M. Gruyters, C. Teodorescu, P. Dumas, Y.J. Chabal, M.C. Asensio, Appl. Surf. Sci. 123/124 (1998) 156.
[2] R.J. Phaneuf, P.A. Bennett, M. Marsi, S. Gunther, L. Gregoratti, L. Casalis, M. Kiskinova, Surf. Sci. 431 (1999) 232.
[3] K. Hirose, A. Hanta, M. Uda, Appl. Surf. Sci. 162/163 (2000) 25.
[4] C. Grupp, A. Taleb-Ibrahimi, Phys. Rev. B 57 (1998) 6258.
[5] T. Osaka, A. Kodera, T. Misato, T. Homma, Y. Okinaka, O. Yoshioka, J. Electrochem. Soc. 144 (1997) 3462.
[6] W.J. Dauksher, D.J. Resnick, W.A. Johnson, A.W. Yanof, Microelectron. Eng. 23 (1994) 235.
[7] W. Kern, D.A. Puotinen, RCA Rev. 31 (1970) 187.
[8] Y.J. Chabal, G.S. Higashi, K. Raghavachari, V.A. Burrows, J. Vac. Sci. Technol. A 7 (1989) 2104.
[9] G.S. Higashi, R.S. Becker, Y.J. Chabal, A.J. Becker, Appl. Phys. Lett. 58 (1991) 1656.
[10] H.E. Hessel, A. Feltz, M. Reiter, U. Memmert, R.J. Behm, Chem. Phys. Lett. 186 (1991) 275.
[11] H. Gerischer, in: H. Eyring (Ed.), Physical Chemistry: An Advanced Treatise, vol. 9A, Academic Press, New York, 1970, p. 463.
[12] H. Gerischer, Electrochim. Acta 35 (1990) 1677.
[13] G. Oskam, J.G. Long, A. Natarajan, P.C. Searson, J. Phys. D 31 (1998) 1927.
[14] G. Oskam, J.G. Long, M. Nikolova, P.C. Searson, Mat. Res. Soc. Symp. Proc. 451 (1997) 257.
[15] J. Zegenhagen, Surf. Sci. Rep. 18 (1993) 199.
[16] C.P. Wade, C.E.D. Chidsey, Appl. Phys. Lett. 71 (1997) 1679.
[17] C. Rossiter, I.I. Suni, Surf. Sci. 430 (1999) L553.
[18] R. Srinivasan, I.I. Suni, Surf. Sci. 408 (1998) L698.
[19] R. Srinivasan, I.I. Suni, J. Electrochem. Soc. 146 (1999) 570.
[20] G. Oskam, P.C. Searson, Surf. Sci. 446 (2000) 103.
[21] G. Oskam, P.C. Searson, J. Electrochem. Soc. 147 (2000) 2199.
[22] P.M. Hoffmann, A. Radisic, P.C. Searson, J. Electrochem. Soc. 147 (2000) 2576.
[23] I.K. Robinson, Phys. Rev. B 33 (1986) 3830.
[24] J.C. Ziegler, G. Scherb, O. Bunk, A. Kazimirov, L.X. Cao, D.M. Kolb, R.L. Johnson, J. Zegenhagen, Surf. Sci. 452 (2000) 150.
[25] K. Sumitomo, T. Kobayashi, F. Shoji, K. Oura, Phys. Rev. Lett. 66 (1991) 1193.
[26] S.M. Durbin, L.E. Berman, B.W. Batterman, J.M. Blakely, Phys. Rev. B 33 (1986) 4402.